

JUN 04 1993

TITLE DEFLAGRATION-TO-DETONATION IN GRANULAR HMX:  
IGNITION, KINETICS, AND SHOCK FORMATION

AUTHOR(S) J. M. McAfee, M-7, B. W. Asay, M-8 and  
J. B. Bdzil, M-7

SUBMITTED TO 10th International Detonation Symposium  
Boston Park Plaza Hotel and Towers  
Boston, Massachusetts 02116-3912  
July 12-16, 1993

DISCLAIMER

This report was prepared as an account of work sponsored by an agency of the United States Government. Neither the United States Government nor any agency thereof, nor any of their employees, makes any warranty, express or implied, or assumes any legal liability or responsibility for the accuracy, completeness, or usefulness of any information, apparatus, product, or process disclosed, or represents that its use would not infringe privately owned rights. Reference herein to any specific commercial product, process, or service by trade name, trademark, manufacturer, or otherwise does not necessarily constitute or imply its endorsement, recommendation, or favoring by the United States Government or any agency thereof. The views and opinions of authors expressed herein do not necessarily state or reflect those of the United States Government or any agency thereof.

By acceptance of this article, the publisher recognizes that the U.S. Government retains a nonexclusive, royalty-free license to publish or reproduce the published form of the contribution, or to allow others to do so, for U.S. Government purposes.

The Los Alamos National Laboratory requests that the publisher identify this article as work performed under the auspices of the U.S. Department of Energy.

Los Alamos

Los Alamos National Laboratory  
Los Alamos, New Mexico 87545

## DEFLAGRATION-TO-DETONATION IN GRANULAR HMX: IGNITION, KINETICS, AND SHOCK FORMATION

J. M. McAfee, B. W. Asay, and J. B. Dzil  
Los Alamos National Laboratory  
Los Alamos, New Mexico, 87545

Experimental studies and analysis of the deflagration-to detonation transition (DDT) in granular HMX are continued. Experiments performed using a direct-gasless igniter exhibit the same phenomenology as those ignited with a piston. Simple kinetics and mechanics describe the formation of the ~100% TMD plug in terms of competing pressurization processes. A mass-conservation analysis of the experimentally observed structures shows how the low velocities characteristic of convective burning are amplified to shock-wave velocities through non-convective processes.

### INTRODUCTION

In the Ninth Detonation Symposium,<sup>1</sup> we presented a descriptive model of the deflagration-to-detonation transition (DDT) of granular HMX confined in steel tubes. The particular experiments described and analyzed in that paper were ignited by a combustion-driven piston. We have since performed experiments on the same material, igniting directly with a high-temperature gasless igniter instead of a piston. We briefly describe these experiments and correlate the previous analysis with these observations.

Further experimentation and consideration of the observed phenomena, particularly in the region below the plug, have led us to expand and correct the original descriptive model. The nature of the burning in the compacted material is crucial to understanding the observed phenomena. Preliminary discussion on the nature and application of autocatalytic kinetics to this problem is given by McAfee, Asay, and Fern.<sup>2</sup> Here we will expand and modify that exposition and consider ideas about intergranular gas pressure and energy transport in granular beds.

### EXPERIMENTAL RESULTS

The directly ignited experiments were similar to those described by Campbell.<sup>1</sup> The same lot of granular HMX used in the previous studies<sup>1</sup> was hand packed in mild steel tubes (~76-mm outer diameter, 12.7 mm inner diameter) and ignited with the previously described Ti/B/Pyrofuse<sup>®</sup> system. Beginning 13 mm above the igniter, coaxial ionization pins were placed in a double-spiral pattern with a net vertical spacing of 2 mm. Pin response was recorded by time interval meters to an accuracy of 1.3 ns. Some of the steel tubes burst during the tests. Those that did not were axially sectioned and the profile of the inner diameter measured. The terminal observations for all the tests showed similar structures, although the burst tubes were not quantitatively measured. Figure 1(a) shows the pin data and wall profile for Shot No. B 9827.

The expanded-tube profile and pin-report times are plotted *versus* distance from the igniter. The expansion data are an average of the two sides of the axial section. Figure 1(b) shows the incremental velocities (pin separation divided by report-time difference) for pairs of pins in the leading trajectory. The six pins that reported late are plotted, but are not considered for velocity. The pins used in this experiment were not particularly well constructed, and some significant fraction had different threshold behavior, thus the occasionally anomalous report times.

The pin data indicate the transition to detonation occurred at approximately 52 mm. The tube expansion and inner-bore surface characteristics are consistent with this position for the transition. The expansion measurements are confounded in this area because the axial section passed through two of the pin holes at 50 and 52 mm. There are four regions evident in the wall-expansion data: (i) = 0 to ~10 mm, (ii) = ~10 to ~30 mm, (iii) = ~30 to ~50 mm, and (iv) = ~50 mm to the end of the tube. Region (i) does not have corresponding pin data. The expansion indicates a relatively low pressure. Region (ii) corresponds to an approximately constant velocity front as measured by the incremental velocities, and the pressure increases moderately. Region (iii) indicates rapidly increasing pressure, and the pins show a rapid increase in velocity. In region (iv), the reduced expansion is typical, not significant, and due to confinement loss near the end of the tube. The last four pins give the detonation velocity of the original density material.

The incremental velocities indicate the tube profile in regions (iii) and (iv) is each composed of two distinct velocity regimes. In region (iii), the velocities increase rapidly from less than 1 km/s to over 9 km/s in slightly over a 10 mm distance. In fact, the last velocity (9.13 km/s) is marginally above the detonation velocity of Theoretical Maximum Density (TMD) HMX.<sup>3</sup> Even though this velocity is determined by only two pin reports, it clearly is not the beginning of a detonation because the next velocity up the tube is much less, constant, and spans three pins. As stated in Reference 1, we attribute this sort of velocity to inappropriately connecting data points from regions with distinctly

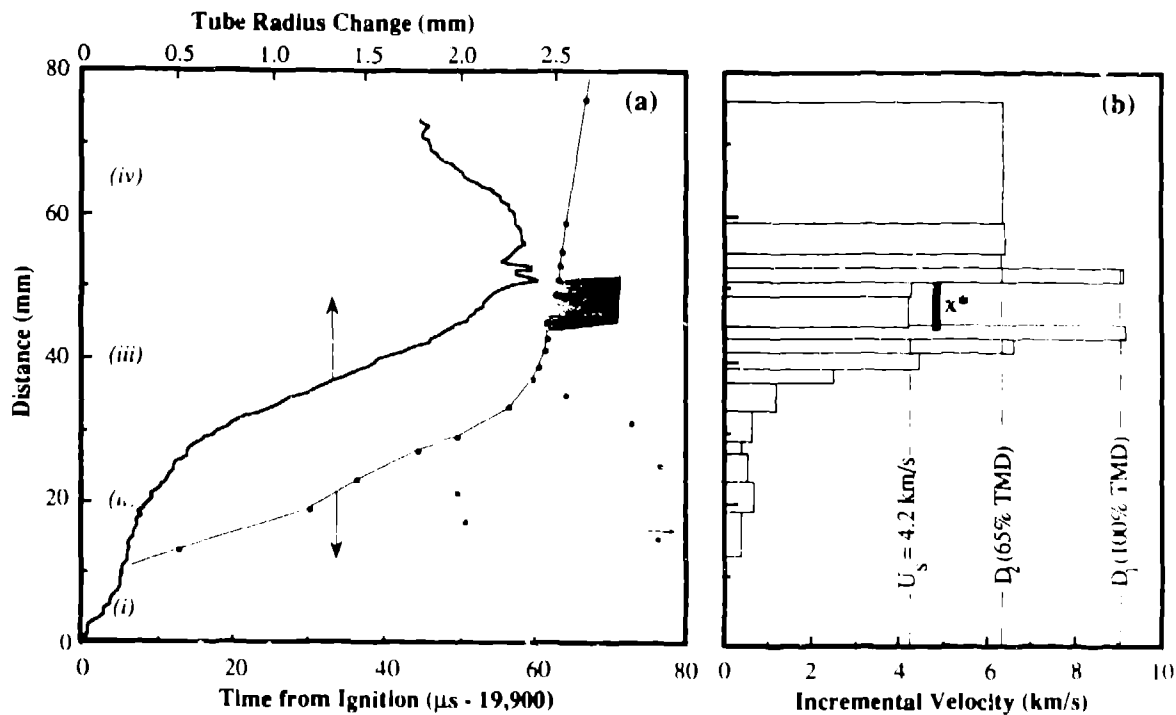


FIGURE 1. TUBE PROFILE, PIN RECORD, AND INCREMENTAL VELOCITIES FOR SHOT NO. B-9827.

different physical properties and histories. Our model of the DDT process postulates a contact-surface discontinuity between a burning region and a near 100% TMD region we have identified as the plug. These current data are interpreted by this model. The region immediately above this discontinuity (velocity = 4.2 km/s) corresponds to the shock that is the upper boundary of the plug. The region below the discontinuity is reacting rapidly and is described by a locus of a fixed (but arbitrary) amount of reaction in the approximately 90% TMD compact. The amount of reaction for this particular locus is determined by the threshold behavior of the diagnostic pins.

It is informative to compare the pin-measured 6-mm run distance of the 4.2-km/s shock and the run-to-detonation ( $x^*$ ) derived from the full-density HMX Hugoniot and Pop Plot<sup>4</sup> for that velocity. The calculation results in a shock pressure of 5 GPa and an  $x^*$  of 6.5 mm. This value of  $x^*$  is plotted on the incremental velocity-distance graph in Fig. 1.

Region (iv) exhibits a two-pin incremental velocity of 9.09 km/s, followed by a four-pin velocity equal to the detonation velocity of 65% TMD HMX (6.4 km/s). The detonation, initiated in the compact, overtakes the initial compaction wave, and subsequently proceeds (more slowly) in original density material. The observation of these two distinct detonation velocities indicates the existence and position of a compaction

wave in these directly ignited experiments, the same as for the piston-ignited experiments.<sup>1</sup>

## DISCUSSION

### Ignited Experiments

One of the continuing controversies in descriptions of the DDT is the significance of convective combustion (See citations in Reference 1). By definition, convective combustion requires the net velocities of the two (or more) phases be different. Our previous experiments using piston-driven ignition, by their very nature, compacted the bed before ignition or any of the structures required for transition to detonation were established. The initial piston compaction of the granular bed to approximately 90% TMD essentially eliminated the possibility of significant gas flow relative to the solid matrix in scales larger than a grain size.

The current ignition-started experiments remove the constraint of precompaction by piston motion. However, the phenomenology observed is the same as for the piston-started experiments. Undoubtedly, the very early stages of burning in ignited experiments are convective. The pressures, Reynolds numbers, and gas evolution rates are small enough that gas can flow through the initial bed. However, the gas permeation into the nascent bed is limited. For those materials that can transit to detonation, the burning rate is high enough

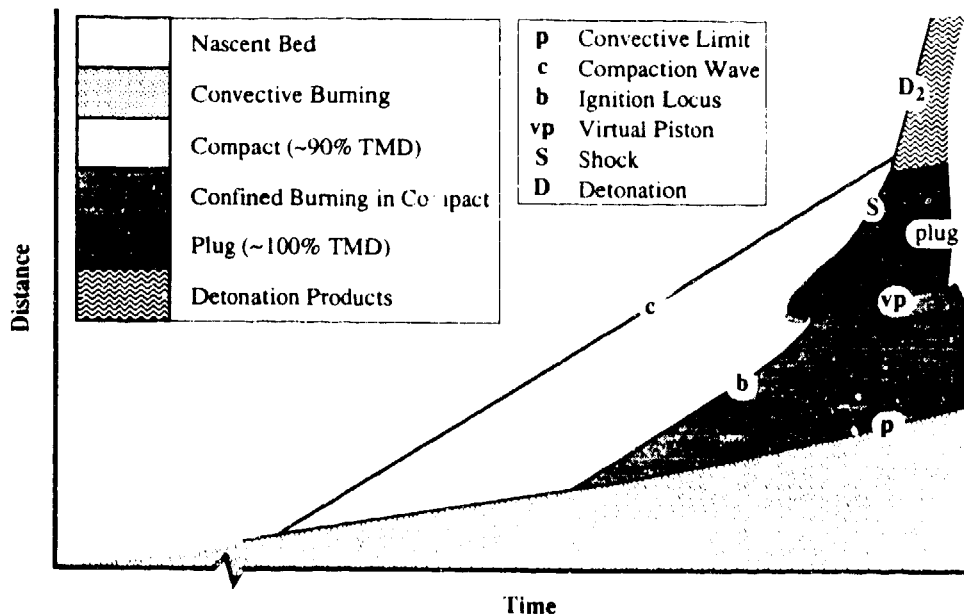


FIGURE 2. SCHEMATIC OF THE DDT PROCESS IN GRANULAR HMX.

that product gas is produced faster than it can flow away. The subsequent build-up of pressure and the resulting compaction of the bed are well described by Campbell.<sup>3</sup> By placing diaphragms at various distances in the HMX bed, Campbell determined that convection was significant for only the first 10 to 15 mm. Additionally, Asay and others<sup>5</sup> have ignited granular HMX below a confined bed of SiC particles of similar size distribution and porosity as the nascent HMX bed. Measurements of the pressure at stations within the effectively-rigid bed indicate bulk gas penetration at a velocity on the order of only 10 m/s for driving pressures of approximately 0.3 GPa. Therefore, convection in beds of these porosities is too slow to have anything but a slight influence on the higher-velocity trajectories and long ignition-time phenomena observed in both piston- and ignition-driven experiments.

The wall profile of region (i) in Fig. 1 indicates a build-up of pressure over an approximately 10-mm distance. The small expansion of the wall indicates this region was exposed to the lowest pressure in the bed. We believe the important effects of convection in these DDT experiments are confined to this relatively short region. Once the gas generation rate is sufficient to overcome convective losses, the flow is choked and pressure builds, compacting the bed above the convection limit.

The pin and wall expansion data in regions (ii), (iii), and (iv) are completely consistent with the data and phenomenology presented for piston driven experiments.<sup>1</sup> Therefore, the boundary between the

low-pressure convective region and the compact is equivalent to a combustion-driven mechanical piston.

#### Descriptive Model

In Fig. 2, we present a schematic of the DDT process for ignited HMX. There are three differences between this diagram and that given in Reference 1: The initial convective region is included, the early-time plug is rounded in shape and somewhat diffuse, and no coalescing stress waves are drawn. Only the last of the three changes is significant. Consideration of the dispersive and dissipative nature of porous beds convinces us that acoustic propagation and subsequent coalescence of characteristics are not an accurate description. Instead, we believe the sensitivity to porosity of the local pressurization by reaction product gases, in conjunction with the compaction behavior of the bed (for the time scales of interest), leads to plug formation. We will explore this assertion in some detail after describing the ignition of the compact. The boundary between the initial convective region and the compact is labeled as *p*. This is the same nomenclature used previously to indicate the trajectory of the mechanical piston because the function is the same. The time axis is broken to indicate that the interval from the first ignition to compaction-wave formation is long relative to the events occurring after compact formation.

The thermal decomposition of HMX is autocatalytic.<sup>6</sup> In all autocatalytic decompositions, there must be a source for the initial product concentration  $x_0$ . We assert  $x_0$  is, in some way, proportional to the strength of the compaction wave (i.e., the work performed on the bed)

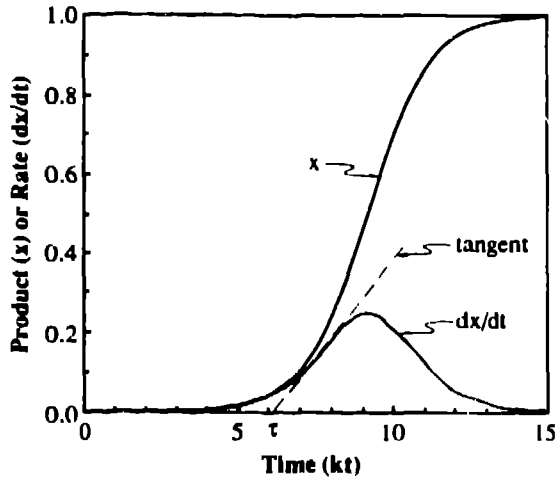


FIGURE 3. PRODUCT CONCENTRATION AND RATE FOR THE SIMPLE AUTOCATALYTIC REACTION. THE INDUCTION PERIOD IS DEFINED BY THE TANGENT TO THE RATE CURVE.

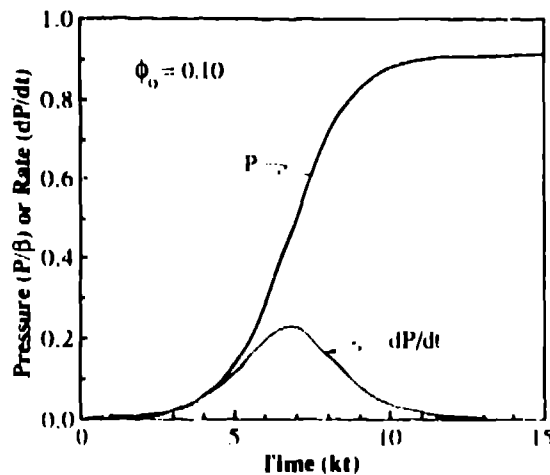


FIGURE 4. THE INTERGRANULAR PRESSURE AND RATE FOR AN INITIAL POROSITY OF 0.10.

The compaction wave provides the energy for the initial decomposition by shear, compression, and friction. The experimental observations reported in Reference 1 show faster pistons give shorter induction periods, therefore the time between compaction and ignition,  $\tau$ , depends inversely on  $x_0$ . This dependence can be estimated for autocatalytic kinetics. Taking the rate of reaction proportional to the concentration of both the reactant and the product, for the general decomposition of reactant A into product X is



For  $n = 1$ , the simple autocatalytic rate law and its integral are

$$\frac{dx}{dt} = kax = k(a_0 - x)(x + x_0) \quad \text{and}$$

$$kt = \frac{1}{(a_0 + x_0)} \ln \frac{a_0(x_0 + x)}{x_0(a_0 - x)} \quad (2)$$

where  $k$  is the rate constant,  $a$  and  $x$  are concentrations at time  $t$ ,  $a_0$  and  $x_0$  are initial concentrations, and  $x$  is the progress variable. The total product concentration is  $x = x_0 + x(t)$ . Initially ( $t = 0$ ),  $x = 0$  and  $a = a_0$ , while at the final equilibrium ( $t \rightarrow \infty$ ),  $x \rightarrow a_0$  and  $a \rightarrow 0$ .

Some of the properties of this rate law, particularly the induction period, are detailed in Reference 2. The induction time is defined by the abscissa-intersection of the tangent to the rate curve as shown in Fig. 3. (As an example, we choose  $x_0 = 0.0001$  for this and the following graphs.) The induction period  $\tau$  depends primarily on the rate constant and the initial product concentration  $x_0$ , because for cases of interest, the initial product concentration is small,  $x_0 \ll a_0$ , and  $a_0 = 1$ .

$$k\tau = \frac{1}{(a_0 + x_0)} \left[ \ln \left( \frac{a_0(2 - \sqrt{3})}{x_0} \right) - \sqrt{3} \right] \quad (3)$$

The rate  $dx/dt$  at time  $\tau$  is approximately 0.18 of the maximum rate. The value for  $x(\tau)$  is 0.045. For this kinetics model, the rate-curve shape is nearly independent of initial product concentration after the induction time. That is, once the induction time is reached and the "fast burning" starts, reaction-rate time histories are similar regardless of the initial product concentration. Therefore, the ignition line **b** in Fig. 2 is not a propagating wave with a distinct boundary, but a locus of constant reaction rate or product concentration. Experimental measurements of the ignition locus have often incorrectly been associated with convective burning.

We can estimate the interstitial pressure  $P$  in the compact due to reaction products using the ideal gas law and assuming incompressible solid.

$$P = \beta \frac{x}{x + \phi_0} \quad \beta = \frac{\rho_0 RT}{M} \quad (4)$$

where  $\phi_0$  is the initial porosity,  $\rho_0$  the initial solid density,  $R$  the gas constant,  $T$  the absolute temperature, and  $M$  the average molecular weight of the products. The pressure history is similar in shape to the product concentration. The interstitial pressure and its time derivative (the pressure rate,  $dP/dt$ ) are graphed in Fig. 4 for an initial porosity of 0.10. Comparison with Fig. 3 shows  $P$  and  $dP/dt$  lead  $x$  and  $dx/dt$  by approximately  $2.2kt$  for these conditions.

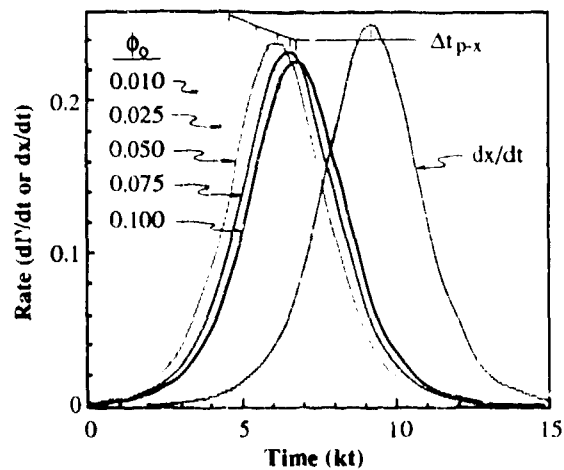


FIGURE 5. PRESSURE RATE AS A FUNCTION OF INITIAL POROSITY.

In Fig. 5 we plot the pressure-rate for several values of the initial porosity for a constant initial product concentration. The amount of time by which the pressure-rate leads the product-concentration rate is a function of  $\phi_0$ . By taking the proper time derivatives and using the above approximations, it is straightforward, though tedious, to show that the time difference  $\Delta t_{p-x}$  between the maximum pressure-rate and the maximum concentration-rate is independent of the initial product concentration. This is plotted in Fig. 6 and given by

$$\Delta t_{p-x} = \ln\{(1 + \phi_0)/\phi_0\}. \quad (5)$$

The interaction of the burn region and the compact can be understood with the help of Figs. 7 and 8. The isobars  $P(b)$  represent the influence of the burning region on the compact and are schematic. They indicate pressure equilibrium behind the ignition locus and their trajectory in the compact above  $b$ . Pressure generated in the burning region (below  $b$ ) propagates into the bed (above  $b$ ). At the same time, low levels of product in the compact (derived from the decomposition started by the compaction wave) provide intergranular pressure to resist further compaction. This is represented by the isobars  $P(c)$  plotted as dotted lines parallel to and earlier than  $b$ . The final pressure stress field for a given location is a superposition of  $P(c)$ ,  $P(b)$ , and the intergranular stress,  $\sigma_c$ . As the product concentration continues to slowly rise, the intergranular pressure above  $b$  can temporarily keep pace with the rapidly increasing pressure transmitted from the burning region because the intergranular pressure leads the product concentration (Fig. 8). The variation of this time difference with compaction state provides a mechanism that tends to prevent further collapse of the bed. Eventually, one of two events will occur: The compaction initiated reaction will transit to fast burning (i.e., the particle will pass through the  $b$  locus). Or, the rapidly increasing pressure from below  $b$  will overcome the combination of

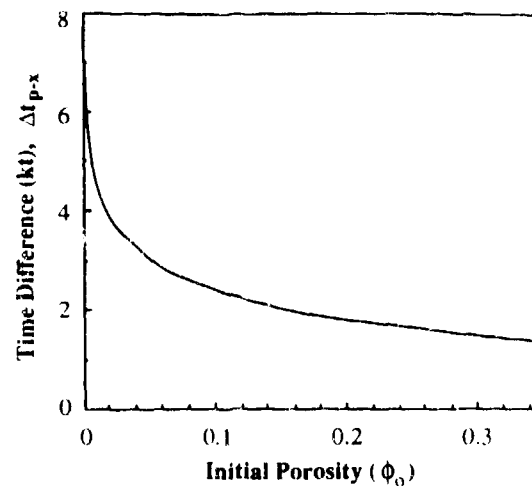


FIGURE 6. TIME DIFFERENCE BETWEEN MAXIMUM PRODUCT RATE AND MAXIMUM PRESSURE RATE.

intergranular stress and product pressure, and the bed will further collapse to a compaction state consistent with the burn region's pressure (i.e., the plug will form).

Which eventuality is determined by the length of time the particle has had to react after compaction and before being affected by the pressure from the burn region. Lower particles (e.g., the  $i^{\text{th}}$  in Fig. 7) have a sufficient portion of their induction time unaffected to produce enough product, and therefore pressure, to prevent further compaction until rapid burning starts. The higher particles ( $j^{\text{th}}$ ) are intercepted sooner after compaction by pressures generated from the burning region. Therefore, there is insufficient intergranular pressure to stop further compaction, and collapse occurs.

Schematically, Fig. 8 shows the intergranular stress and pressure histories of two such particles. For the  $i^{\text{th}}$  particle, the stress generated from the compaction wave  $\sigma_c$  is largely supported by the solid matrix. The product gas pressure  $P(c)$  increases soon enough to resist compaction by the pressure from the burn region  $P(b)$ . The ignition locus  $b$  is reached and the  $i^{\text{th}}$  particle becomes part of the burn region.

For the  $j^{\text{th}}$  particle,  $P(b)$  begins to affect the compact before there is sufficient product pressure to stiffen the bed. The rapid increase in pressure overcomes the combination of solid stress and low intergranular pressure, and compacts the bed further. This additional compaction quenches the decomposition, thus preventing further product evolution.

The experimental evidence clearly indicates the acceleration of the ignition locus, as we have discussed elsewhere.<sup>1,2</sup> We believe that the accelerating ignition locus combines synergistically with the pressurization

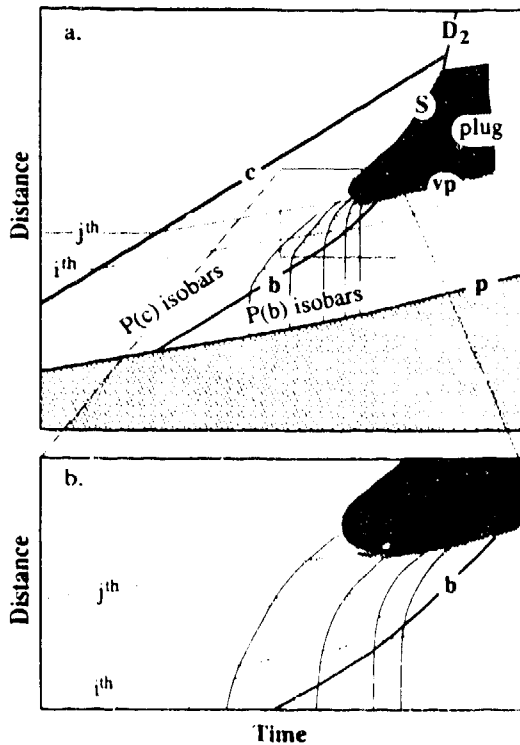


FIGURE 7. PARTICLE PATHS SHOWING THE TIMING OF PRESSURE INTERACTIONS FOR PLUG FORMATION.

density effects to generate the plug. High velocities for the ignition locus below the virtual piston ( $\sim 6.5$  km/s in Fig. 1) can be thought of as providing a near constant-volume ignition of the compact in the vicinity the plug. The pressure will therefore grow rapidly, quickly accelerating the virtual piston and thus forming and accelerating the shock.

At compactions near TMD, the gas phase and gas-producing reactions stop because there is essentially no free volume and the increase in thermal conduction rapidly cools the residual gas. Even deconsolidative burning is slowed by more than an order of magnitude.<sup>1</sup> Therefore, the ignition locus effectively terminates when it intersects the plug. Further reaction of the plug region is governed by condensed-phase kinetics appropriate to shock-induced reactions.

#### Velocity Amplification

The compaction, ignition, and plug formation processes are the mechanisms that generate shock level velocities in this system. Convective burning kinetics and compaction properties of the bed will determine the compaction wave velocity  $u_c$  relative to the convective limit interface velocity  $u_{vp}$ .<sup>1</sup> Mass balance gives

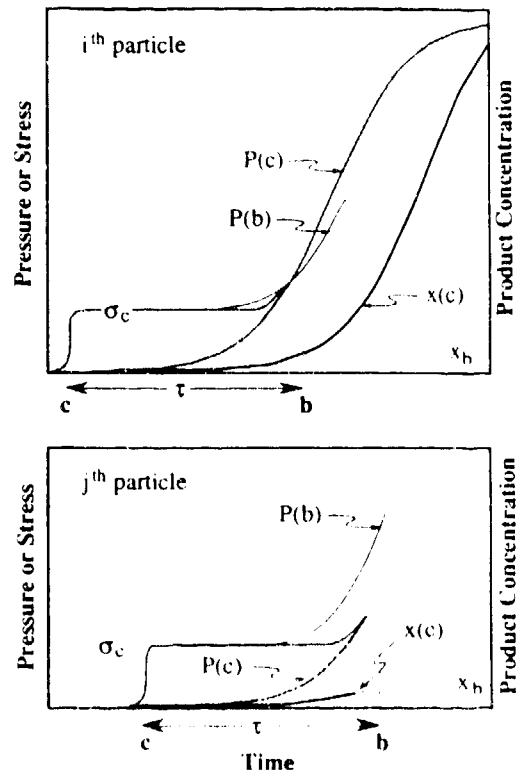


FIGURE 8. PRESSURE, STRESS, AND PRODUCT CONCENTRATION PROFILES FOR THE TWO PARTICLE.

$$u_c = \rho_c / (\rho_c - \rho_0) u_{vp} \quad (6)$$

where  $\rho_c$  is the compact density and  $\rho_0$  the nascent bed density. Because the ignition locus  $b$  follows from the compaction wave  $c$ , the reactive velocity in the system is amplified from tens of m/s (characteristic of convection) to hundreds of m/s.

Amplification of velocities from the order of  $u_c$  to shock speeds can also be estimated using mass balance across  $S$ . Using eq. (6), we rewrite the equation given in Reference 1 as

$$U_s = \rho_s u_{vp} / (\rho_s - \rho_c) u_c \quad (7)$$

where  $U_s$  is the shock velocity,  $\rho_s$  is the plug density ( $\sim 100\%$  TMD), and  $u_{vp}$  is the virtual piston velocity. The shock velocity relative to the virtual-piston velocity is largely determined by the denominator (nominally  $\sim 0.1$ ). This is the amplification necessary to reach shock speeds of km/s, enough for a shock to detonation transition (SDT). There is no direct measurement of  $u_{vp}$ , but the current experimental results for  $U_s$  and  $u_c$  indicate that  $u_{vp}$  is on the order of  $u_c$ .

## CONCLUSIONS

We have shown, using detailed experimental observations, simple mechanics and kinetics, that the transition from deflagration to detonation in granular HMX is a straightforward consequence of material and porous-bed properties. Convective flow and hot-gas ignition contribute only to the early-time, low-velocity phenomena. The formation of a compaction wave in undisturbed material begins the series of non-convective events that lead to a final shock-to-detonation.

This model demonstrates the necessity of a rapid pressurization in the initial bed. The pressurization rate ( $dP/dt$ ) must be large enough such that product gasses cannot infinitely diffuse into the granular bed. With strong enough confinement, the flow is choked because of limited permeability, and the bed above this burning is compacted. The launching of a compaction wave above the convectively-ignited and burning region is the first velocity amplification in the process. The second amplification involves the formation and acceleration of the plug, and is sufficient to reach shock velocities.

We believe this scenario and analysis generally describe the DDT in granular and porous materials. The lack of convective phenomena after compaction leads us to speculate that computational modeling of this and similar systems can be accomplished by invoking the complexity of multi-phase flow only in the precompaction regimes. Therefore, two- and three-dimensional models of the deflagration-to-detonation transition may be computationally within reach in the near future.

## REFERENCES

1. McAfee, J. M., Asay, B. W., Campbell, A. W., and Ramsay, J. B., "Deflagration to Detonation in Granular HMX," Ninth Symposium (International) on Detonation, Portland, OR, 1989, pp. 265-278.
2. McAfee, J. M., Asay, B. W., and Ferm, E. N., "Deflagration to Detonation in Granular HMX: Structure and Kinetics in the Predetonation Region," 1991 JANNAP Propulsion Systems Hazards Subcommittee Meeting, Albuquerque, NM, 1991.
3. Campbell, A. W., "Deflagration-to-Detonation Transition in Granular HMX," 1980 JANNAP Propulsion Systems Hazards Subcommittee Meeting, Monterey, CA, 1980, pp. 105-130.
4. Gibbs, T. R. and Popolato, A., LASL Explosive Property Data, University of California Press, Berkeley, CA, 1980, pp. 42-51.
5. Asay, B. W. and Laabs, G. W., Los Alamos National Laboratory document, M-8-QR-92-4, 1992. or Chitanvis, C. Z., Bdzil, J. B., and Asay, B. W., "The Permeation of High-Pressure Gas Through a Porous Bed," to be published.
6. Rogers, R. N. and Janney, J. L., "Thermochemical Evaluation of Zero-Order Processes Involving Explosives," *Proceedings of the Seventh International Conference on Thermal Analysis*, Vol. II, Chichester, GB, 1981, p. 1434.
7. Fifer, R. A. and Cole, J. E., "Transition from Laminar Burning for Porous Crystalline Explosives," *Seventh Symposium (International) on Detonation*, Annapolis, MD, 1981, pp. 164-174.